ELSEVIER

Contents lists available at ScienceDirect

Microporous and Mesoporous Materials

journal homepage: www.elsevier.com/locate/micromeso



Fabrication of zeolite/polymer composite membranes in a roller assembly



Bo Wang, Eric A. Jackson, Jerry W. Hoff, Prabir K. Dutta*

Department of Chemistry and Biochemistry, The Ohio State University, 100 West 18th Avenue, Columbus, OH 43210, USA

ARTICLE INFO

Article history:
Received 21 September 2015
Received in revised form
16 October 2015
Accepted 4 November 2015
Available online 14 November 2015

Keywords: Bendable zeolite membrane Faujasite Roll-to-roll fabrication CO₂ capture Gas separation

ABSTRACT

Membranes are cost-effective solutions for many industrial separations. Polymer membranes are widely used in gas separations. Because of the solubility-diffusion mechanism of transport, the permeance and selectivity of polymer membranes are inversely related, and is considered a limitation. Zeolite membranes do not have this limitation, but zeolite membrane synthesis is a batch process with long synthesis times and presence of defects. The resulting high costs of manufacture make zeolite membranes noncompetitive for most applications. In this study, we present a roll-to-roll method for zeolite synthesis on a polymer support exploiting a gel that leads to rapid zeolite crystallization and a bendable zeolite membrane structure. Membranes were grown under both compressive and tensile stress, and with zeolite structure both on top and within the pores of the polyethersulfone (PES) support. The structure of the membranes was evaluated by electron microscopy. Membranes were coated with a thin layer of polydimethylsiloxane, and evaluated for CO₂/N₂ separation, relevant for CO₂ capture from flue gas of power plants. As long as the zeolite membrane is grown within the PES support, highly reproducible CO₂/ N_2 separation performance with CO_2 permeance of 1881 \pm 204 GPU and CO_2/N_2 selectivity of 34 \pm 4 was observed immaterial of the stress conditions under which it was grown. For zeolite membrane grown on top of the PES support, the compressive stress resulted in crack formation, with poor transport properties. Demonstration of zeolite membrane fabrication with roll-to-roll method has the potential for industrial level scale up.

© 2015 Elsevier Inc. All rights reserved.

1. Introduction

Polymer membranes are cost effective platforms for a wide variety of gas separations, and in particular in carbon sequestration applications [1]. With increase in gas permeance, there is typically a decrease in selectivity for polymer membranes (Robeson limit) [2]. Inorganic zeolite membranes do not have this limitation. Computational studies have noted that faujasitic zeolite with pore size of 7.4 Å can have CO_2/N_2 selectivity higher than 500 and CO_2 permeability of 10,000 Barrer (1 Barrer = 3.35×10^{-16} mol m/ (m² s Pa)) considerably better than polymeric membranes [3]. Because of their unique gas separation performance, zeolite membranes have been an active research area [4–7]. However, application of zeolite membranes on a commercial scale is limited to only one application, that of ethanol pervaporation, because of

their high cost [5]. Most zeolite membrane research is focused on the laboratory scale.

Polymer membranes have low manufacturing costs because of the roll-to-roll fabrication process [8]. Roll-to-roll process has also been applied for nanoparticle alignment on membrane support and pattern printing on films [9–12]. However, roll-to-roll fabrication method has never been applied in zeolite synthesis, because conventional zeolite synthesis takes long time and with the typical rigid alumina supports, roll-to-roll technology cannot be used [5].

Our group has reported methods to decrease zeolite crystallization time, synthesize zeolite membranes on polymer supports and fabricate bendable zeolite membranes [13–16]. A dehydration/rehydration strategy was developed to decrease the synthesis time of faujasitic zeolites with crystallization times of <2 h, and this time scale is potentially applicable for roll-to-roll synthesis. With this method, flat-sheet zeolite membranes were synthesized and examined for CO_2/N_2 gas separation [14]. A bendable zeolite membrane concept was developed by growing zeolite layer only within a polymer membrane [15]. The gas separation property was maintained after bending to a certain curvature.

Corresponding author.

E-mail address: dutta@chemistry.ohio-state.edu (P.K. Dutta).

In this study, a roll-to-roll synthesis setup for zeolite membrane growth within a polymer has been designed and applied for membrane growth. Membranes were characterized with X-ray diffraction (XRD), scanning electron microscopy (SEM) and CO_2/N_2 gas separation. This study demonstrates the potential of producing zeolite membranes in similar fashion to polymeric membranes.

2. Experimental section

2.1. Chemicals

Ludox HS-30 colloidal silica (SiO₂, 30%), aluminum isopropoxide $(Al(O-CH(CH_2)_2)_3,$ 98%), tetramethylammonium ((CH₃)₄NBr, 98%) and Ludox SM-30 colloidal silica (SiO₂, 30%) were purchased from Aldrich (Milwaukee, WI, USA). Aluminum hydroxide (Al(OH)₃, 76.5%) was purchased from Alfa Aesar. Tetramethylammonium hydroxide ((TMAOH), 25% aqueous solution) was purchased from SACHEM Inc. Sodium hydroxide (NaOH, 99.0%) was purchased from Fisher Scientific. Dehesive 944 Polydimethylsiloxane (PDMS) was provided by Wacker Silicones, Inc. Helium (4.5 grade), carbon dioxide (4.0 grade) and nitrogen (4.5 grade) were purchased from Praxair. Polyethersulfone (PES) 300 kDa membrane was purchased from MILLIPORE Biomax. H₂O used in this study was purified by a Millipore ultrapure water system. All chemicals were used as received without further purification.

2.2. Zeolite membrane synthesis with roll-to-roll setup

Zeolite Y Nanoparticle Synthesis Nano sized zeolite Y seeds were synthesized according to literature with composition of 0.048 Na₂O:2.40(TMA)₂O(2OH):1.2(TMA)₂O(2Br):4.35SiO₂:1.0Al₂O₃:249 H₂O, where TMA⁺ is tetramethylammonium cations [17]. Briefly, 26.2 g Ludox HS-30 and 10.46 g TMAOH were mixed in a sealed bottle and stirred at room temperature for 30 min. 12.5 g aluminum isopropoxide was dissolved in mixture of 76.5 g H₂O and 52.3 g TMAOH solution, and heated in a water bath at 70 °C until complete dissolution. After cooling to room temperature, 13.1 g TMABr was added to alumina source solution followed by mixing with the silicon source. The clear sol was aged at room temperature with stirring for 3 days and then in an oil bath at 100 °C for 4 days. After synthesis, nanozeolite particles were separated by ultracentrifugation (using Sorvall MX and Beckman Coulter Allegra 64RD centrifuges), and washed until pH of supernatant was 7. Purified nanozeolite seed dispersion was stored as a 1 wt% aqueous stock solution.

Deposition of Zeolite Y Nanoparticle on PES support Nanozeolite seed particles were deposited on PES supports by vacuum assisted dip-coating. PES supports were soaked in distilled water overnight and then in isopropanol for 1 h before washing with water again. Nanozeolite dispersion was ultra-sonicated for 1 h and diluted with distilled water to the required concentration. About 20 mL of nanozeolite suspension was placed in petri dish. The PES support was dipped in the petri dish for 3 s, A ~25 psi vacuum was applied on the back of the PES support to pull the seeds onto the support. After coating, the support was dried at room temperature overnight and stored in plastic sample bags.

Roll-to-Roll Synthesis Setup The roll-to-roll synthesis setup designed in this study is shown in Fig. 1. This setup consists of 4 parts: rollers, reactor, temperature controller and a rehydration assembly. Two identical motor rollers and one fixed column all of diameter of 5.1 cm was used. Nonwoven fabric band was affixed to the rollers and fixed column, and could be moved with adjustable rolling speed. Temperature controller consists of a thermocouple, a digital temperature controlling box and four 100 W heaters placed in the holes at the bottom of the reactor. The reactor temperature is

set at 100 $^{\circ}\text{C}$. Rehydration of gel was realized by continuous addition of water from a burette.

Roll-to-Roll Synthesis of Zeolite Membranes Gel composition used in the reactor is: 8.3 Na₂O:1 Al₂O₃:6.4 SiO₂:483.9 H₂O. After dissolving 4.416 g of Al(OH)₃ and 14.58 g NaOH in 170.48 g H₂O, 27.7 g Ludox SM-30 was added to the gel. Mixed gel was sealed in polypropylene bottle and aged at room temperature for 4 h. Aged gel was transferred to a dehydration/rehydration hydrothermal setup for removal of half the water in 1 h. This partially dehydrated hot gel was then immediately transferred to the reactor shown in Fig. 1 and heated to 100 °C. Seeded PES support was stapled onto the outer side of rolling non-woven fabric band. Entire PES support was immersed into the gel in the beginning of zeolite growth. During 1 h of zeolite growth process, water was added to the gel, diluting the gel from 120 mL to 200 mL. At the same time, PES support moved through the gel due to movement of the rolling non-woven fabric via the rollers. After zeolite growth, membrane sample was washed with flowing water and rubbed with a fur brush, soaked in water to remove residual surface species and dried for further study.

2.3. Polydimethylsiloxane (PDMS) coating

Zeolite membranes were spin coated with PDMS (Dehesive 944 kit) before gas separation test. Commercial PDMS comes in 3 separate bottles, containing PDMS monomer, catalyst and cross-linker (the exact nature of these chemicals is proprietary, and the procedure followed was supplied by the vendor). First, PDMS monomer solution was diluted with heptane. After complete dispersion, cross linker and catalyst were added with the ratio of 100:1:0.5 (PDMS: Cross linker: Catalyst) to prepare PDMS precursor solution. Before spin coating, zeolite membrane sample was taped on a spin coating support, which provides mechanical stability in spinning process. PDMS precursor solution was dropped to cover entire membrane surface area, and left for 3 s before spinning. Samples were spun at 2000 rpm for 5 s followed by 4000 rpm for 1 min. After coating, PDMS was polymerized at room temperature overnight.

2.4. Characterization

Bruker D8 X-ray Diffractometer with CuK α ($\lambda=1.5405$ Å) was used to characterize the phase composition of zeolite membranes. FEI Helios Nanolab 600 Dual Beam Focused Ion Beam/Scanning Electron Microscope (FIB/SEM) was employed to characterize surface morphology of zeolite membrane samples.

2.5. Gas separation study

Fabricated zeolite membrane was applied for CO_2/N_2 separation. Gas flow compositions were controlled with a flow box and mass flow controllers from SIERRA Instruments Inc. Feed gas and sweep gas have flow rates of 60 mL/min and 30 mL/min, respectively. Compositions of permeate and retentate gas were investigated with a SRI 310C gas chromatograph equipped with a Hysep D column and TCD detector.

3. Results

3.1. Synthesis of zeolite membrane

The roll-to-roll synthesis setup shown schematically in Fig. 1a was employed to synthesize zeolite membranes while moving through a heated aluminosilicate gel. Fig. 1b is a picture of this setup. This setup consists of 2 moving rollers, a fixed column

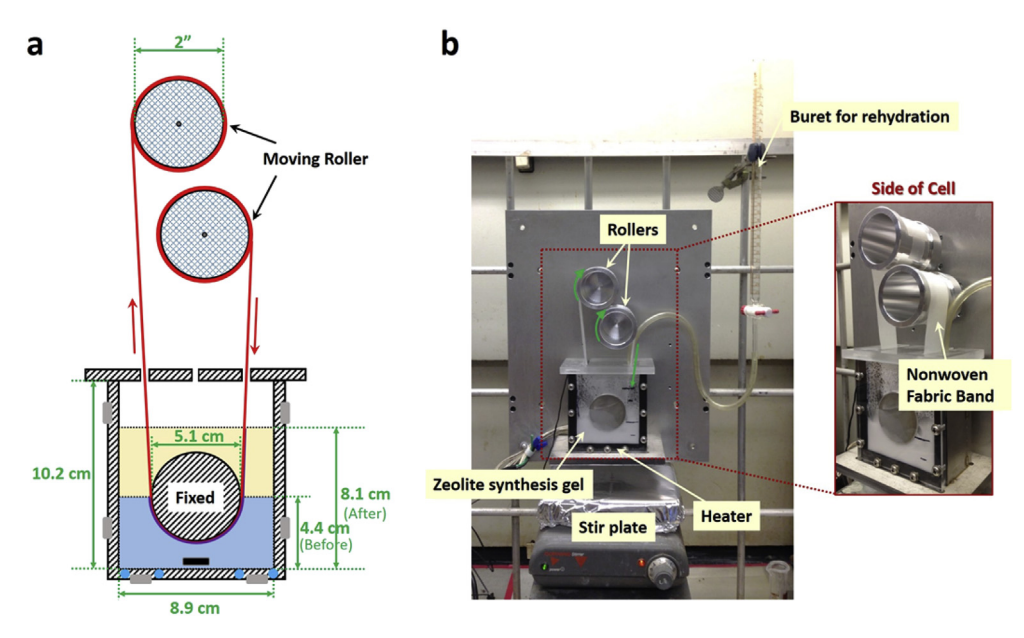


Fig. 1. (a) Scheme and (b) picture of roll-to-roll synthesis setup.

dipping in a reactor containing the aluminosilicate gel, a heater assembly for controlling the temperature of the bath, a stirrer for stirring the gel, and a burette assembly for adding the water back during the synthesis. Rollers and fixed column have diameter of 5.1 cm. Nonwoven fabric band was attached to the two rollers and fixed column as shown in Fig. 1a. During the synthesis process, the two rollers rotate in a clockwise fashion with adjustable speed, so that the nonwoven fabric band moves through the gel from right to left as shown by arrows marked in Fig. 1a. Temperature control is achieved with four 100 W heaters, a thermocouple, and a digital temperature controlling box (Fig. 1b).

Commercial PES (300 kDa) ultrafiltration membranes are chosen as the polymer support. PES consists of a ~100 μm mesoporous PES layer on top of a ~200 μm non-woven fabric [14]. PES layer has average pore size of ~70 nm and a porosity of 15% [14]. Nanozeolite seed particles of 30–40 nm in size were coated into the PES support using vacuum-assisted coating method. Seeded PES support (4 cm \times 2 cm) was stapled onto the band of non-woven fabric, and was rolled during the synthesis process through the reactive aluminosilicate gel.

The synthesis process is schematically shown in Fig. 2a. An aluminosilicate gel of composition of 8.5 Na₂O:1 Al₂O₃:10.9 SiO₂:974 H₂O was prepared, aged, and heated under reflux and 40% of the water is removed to result in a gel of composition 8.5 Na₂O:1 Al₂O₃:10.9 SiO₂:584 H₂O, as described in a previous paper [13]. The hot partially dehydrated gel is transferred into the reactor and totally immerses the PES support, as shown in Fig. 2b, and heated to 100 °C. Initially, the seeded PES support is bent around the 5.1 cm fixed column, and as the crystallization proceeds, and the PES band rolls, zeolite membrane gets slowly flattened. During the hour of roll-to-roll synthesis process, the nanozeolite seeded PES support moves from position "1" to "2" in Fig. 2b. At the same time, volume of zeolite gel increases from 120 to 200 mL because of rehydration of gel via continuous addition of water from burette (Fig. 1b). Final fabricated zeolite membrane was in a flat geometry.

Two different geometries of zeolite growth were explored. Fig. 3 details these geometries. In the first case (convex), the seeded PES side of the support was directly exposed to the hot aluminosilicate gel. As growth occurred over one hour, and the membrane moved from position 1 to 2, the flattening of the membrane will lead to compressive stress, as shown in Fig. 3a, b. Two different nanozeolite

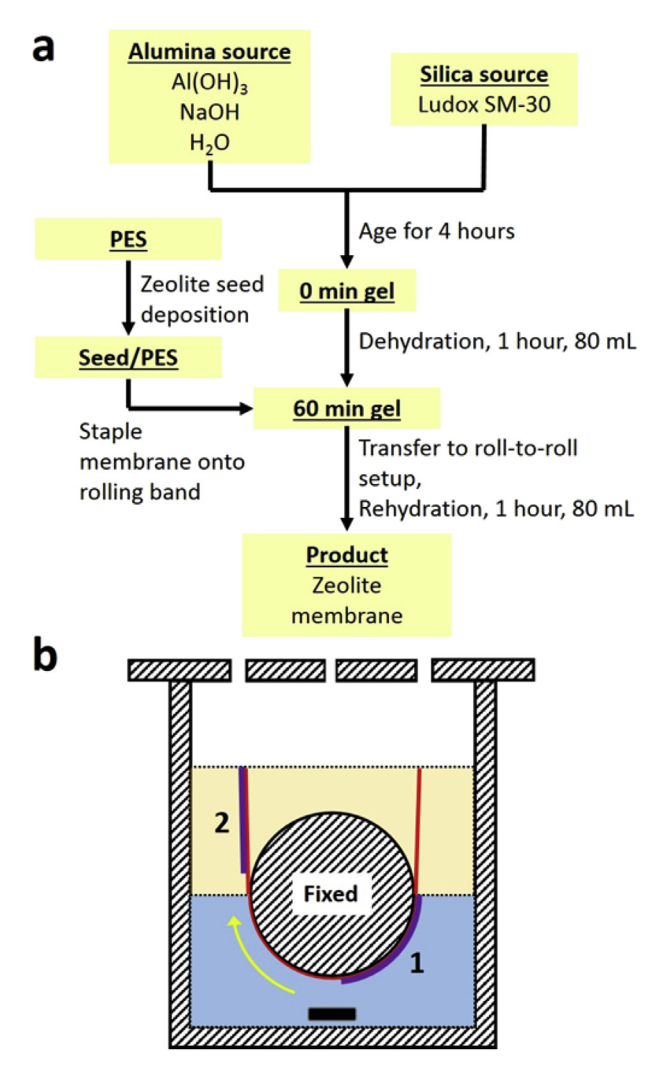


Fig. 2. (a) Synthesis procedure of zeolite membrane and (b) schematic of zeolite membrane synthesis process in roll-to-roll synthesis cell, (1) is the starting position of the seed coated PES on non-woven fabric and (2) is the end position after synthesis is complete.

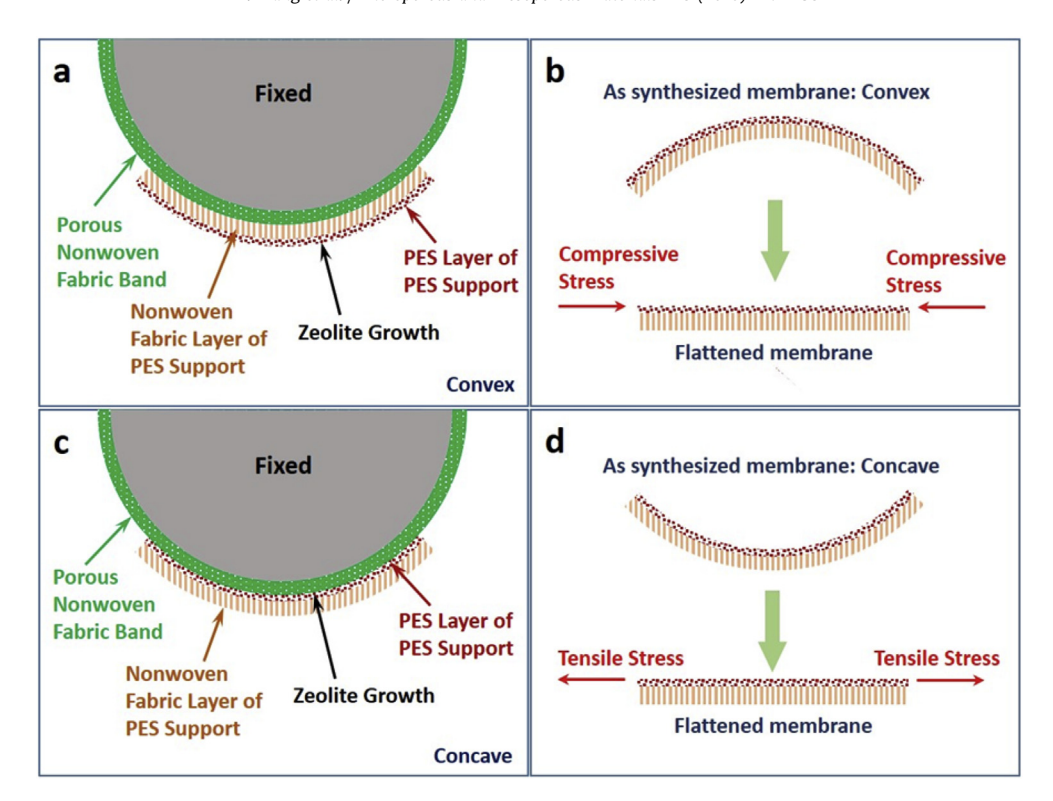


Fig. 3. Scheme of (a) convex and (c) concave synthesis geometries realized in the roll-to-roll reactor, and the type of stress experienced during (b) convex and (d) concave growth and eventual flattening of membrane.

seed loading levels of the PES were examined in this particular geometry (10 and 14 $\mu g/ml$). In the second geometry (concave), the seeded PES layer (10 $\mu g/ml$) faces towards the fixed column, being separated from it by the highly porous non-woven fabric band (which acts as the moving support, as well as letting reactants through). In this case, as the membrane moves from position 1 to 2, upon flattening, the membrane will be subjected to tensile stress, as show in Fig. 3c,d.

3.2. Characteristics of zeolite membrane by roll-to-roll synthesis

The XRD pattern of bare PES support, and membranes synthesized by the three methods are shown in Fig. 4. From the reflections, it is apparent that a zeolite with the faujasite framework is formed on the PES in all cases.

Fig. 5 compares the morphology of the membranes grown in the two geometries for the low seed loading (10 µg/ml) sample. For the concave geometry (Fig. 5a), there are less crystals on the top of the PES membrane as compared to the convex geometry (Fig. 5f). though in both cases the underlying PES matrix is visible, indicating that this top layer is not continuous. In both cases, the PES was dissolved with N-methylpyrrolidone (NMP), and large slabs of interconnected zeolite crystals (cm scale, visible to the naked eye) were found (Fig. 5b and g, note the layer resting on the non-woven fabric). A continuous zeolite layer is being formed within the PES membrane. Fig. 5c and h are higher resolution images of the zeolite layer, and shows that they are made up of small crystals. The side view of the self-standing zeolite films for the two geometries are compared in Fig. 5d,e,i,j. The thickness of the concave membrane is $5 \mu m$, as compared to $3 \mu m$ in the convex case. The zeolite particles making up the inorganic layer are of the order of 100 nm.

For the two films, the exposure to the aluminosilicate gel is significantly different. In the convex film, the PES is in direct contact with the aluminosilicate gel, whereas in the concave film, only the

species that can penetrate through the pores of the non-woven fabric are contacting the seeded PES layer (Fig. 3). This difference explains the presence of more as well as larger crystals on the surface of the convex film, as well as the lower thickness since the gel cover inhibits nutrients from reaching the PES as effectively.

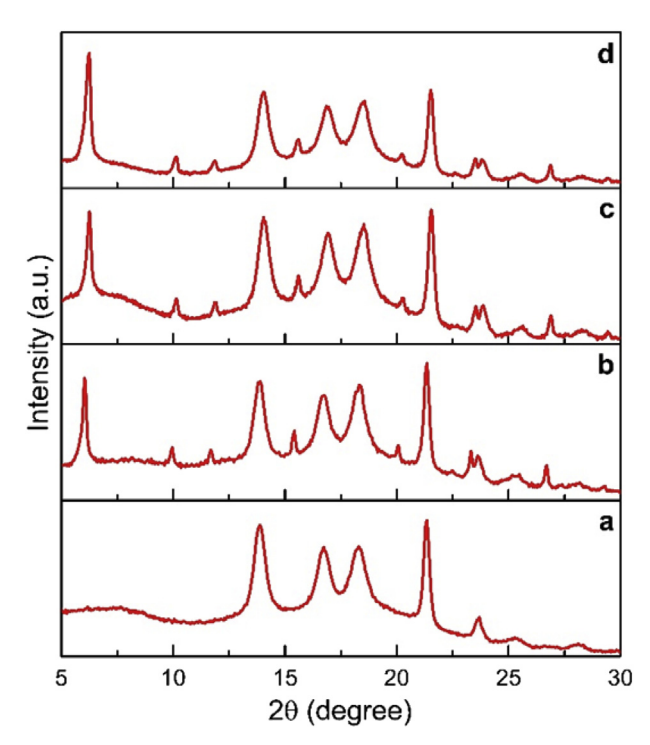


Fig. 4. XRD patterns of (a) bare PES support, (b) convex membrane grown from $14~\mu g/mL$ seeded support, (c) convex and (d) concave membrane grown from $10~\mu g/mL$ seeded support.

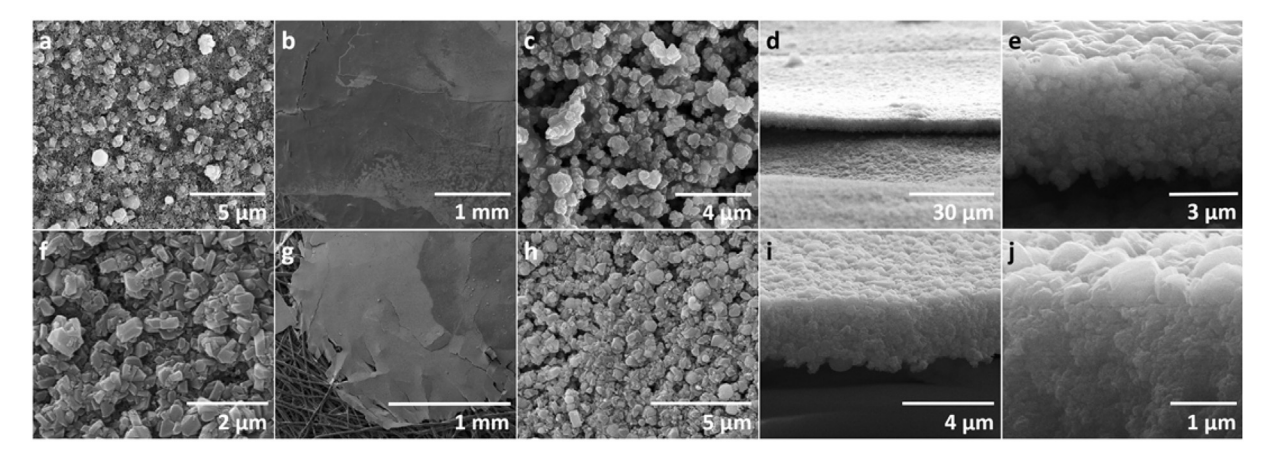


Fig. 5. SEM images of zeolite membranes synthesized with roll-to-roll process with (a–e) concave and (f–j) convex geometries: (a) and (f) are top-view of as-synthesized membranes; (b), (c), (g) and (h) are zeolite films with PES dissolved, with (c) and (h) being of higher magnification; (d), (e), (i) and (j) are side view SEM of zeolite films at different resolutions after PES dissolution.

We also investigated the convex geometry synthesis with a higher loading of nanozeolite seeds in the PES (14 μ g/ml), and the morphology of the as-obtained material is shown in Fig. 6. There is a continuous layer on the surface of well-connected zeolite crystals, and the PES support is not visible (Fig. 6a). At lower magnification, parallel cracks are visible on the membrane (Fig. 6b). Closer inspection of the cracks show that the PES film is intact (Fig. 6c). Upon dissolution, only small pieces of zeolite membrane on the non-woven fabric layer is evident (Fig. 6d).

3.3. CO_2/N_2 separation performance of zeolite membrane by roll-to-roll synthesis

Zeolite/PES membranes fabricated by roll-to-roll synthesis were coated with PDMS (200–300 nm) before examining for CO₂/N₂ separation. Five membrane samples were prepared with concave geometries with low seed loading (10 µg/ml). The CO₂/N₂ separation performance is shown in Fig. 7a, with CO₂ permeance 1881 \pm 182 GPU and CO₂/N₂ selectivity 34 \pm 3. Five samples were prepared with the convex geometry, with CO₂ permeance of 1841 \pm 181 GPU and CO₂/N₂ selectivity of 35 \pm 4. For two samples prepared in the convex geometry with the high loading seed sample (14 µg/ml), the transport properties were CO₂ permeance of 275 \pm 14 GPU and CO₂/N₂ selectivity of 7 \pm 2.

For one of the convex films with the low seed loading, further experiments were carried out. The CO_2/N_2 selectivity increased with CO_2 mole fraction, as did CO_2 permeance, as shown in Fig. 7b. The dependence of the transport properties on temperature of this convex film is shown in Fig. 7c, with both CO_2 and N_2 permeance increasing with temperature, while CO_2/N_2 selectivity decreased. With higher CO_2 mole fraction in feed gas, blocking effect is stronger, so that penetration of N_2 molecules through zeolite pores

is more difficult. Because gas separation is realized by adsorption and diffusion, gas transport rate across the membrane increases with temperature. These observations indicate that the zeolite is responsible for the transport properties.

The mechanical flexing stability of five different sets of the PDMS-coated membranes grown via the low seed convex method was examined. The membranes were bent around different radii of curvature, in the two possible directions, followed by measure of their CO_2/N_2 transport property. These results are shown in Table 1. It appears that the membranes are stable up to bending around 2.5 cm radius in either the bending in or bending out geometry.

One of these convex geometry membranes was repeatedly tested over a period of three days. There was a gradual decrease in permeance of both CO_2 and N_2 (day 1: CO_2 1882 GPU, and N_2 56 GPU; day 2: CO_2 1707 GPU, and N_2 54 GPU; day 3: CO_2 1480 GPU, and N_2 43 GPU), but the CO_2/N_2 selectivity was maintained at 34. This observation of permeance changes is similar to our previous study of membranes grown in a flat geometry [15].

Several control experiments were carried out with the convex geometry membranes. Without the PDMS coating, the CO_2 and N_2 permeance were 2466 and 2096 GPU, respectively, and CO_2/N_2 selectivity of 1. With only PDMS on the PES support, we have reported previously that a CO_2/N_2 selectivity of 14 was observed [15]. In another experiment, PDMS was coated on a seed layer of nanozeolite on PES to mimic a mixed matrix membrane. The CO_2 and N_2 permeance were 607 and 46 GPU, respectively, and CO_2/N_2 selectivity of 12, close to that of a PDMS/PES membrane. Thus, the roll-to-roll grown zeolite membranes coated with PDMS are performing much better than the mixed matrix membrane, which is a collection of zeolite crystals covered with PDMS, similar to results we have previously reported [15].

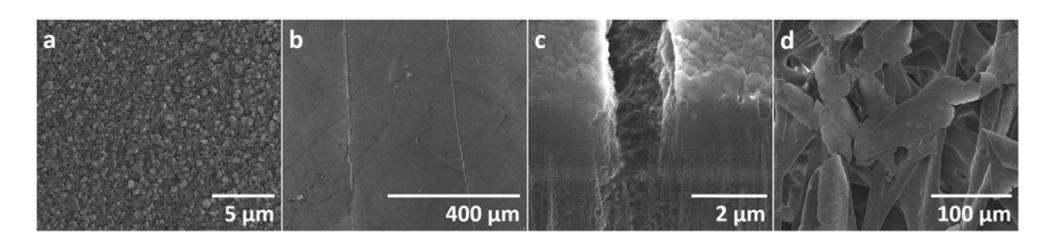


Fig. 6. SEM images of zeolite membranes synthesized with roll-to-roll process in convex geometry with high zeolite seed loading: (a) is top view of as-synthesized membranes; (b) and (c) are top views of cracks on as-synthesized membranes at different magnifications and (d) is zeolite film after PES dissolution.

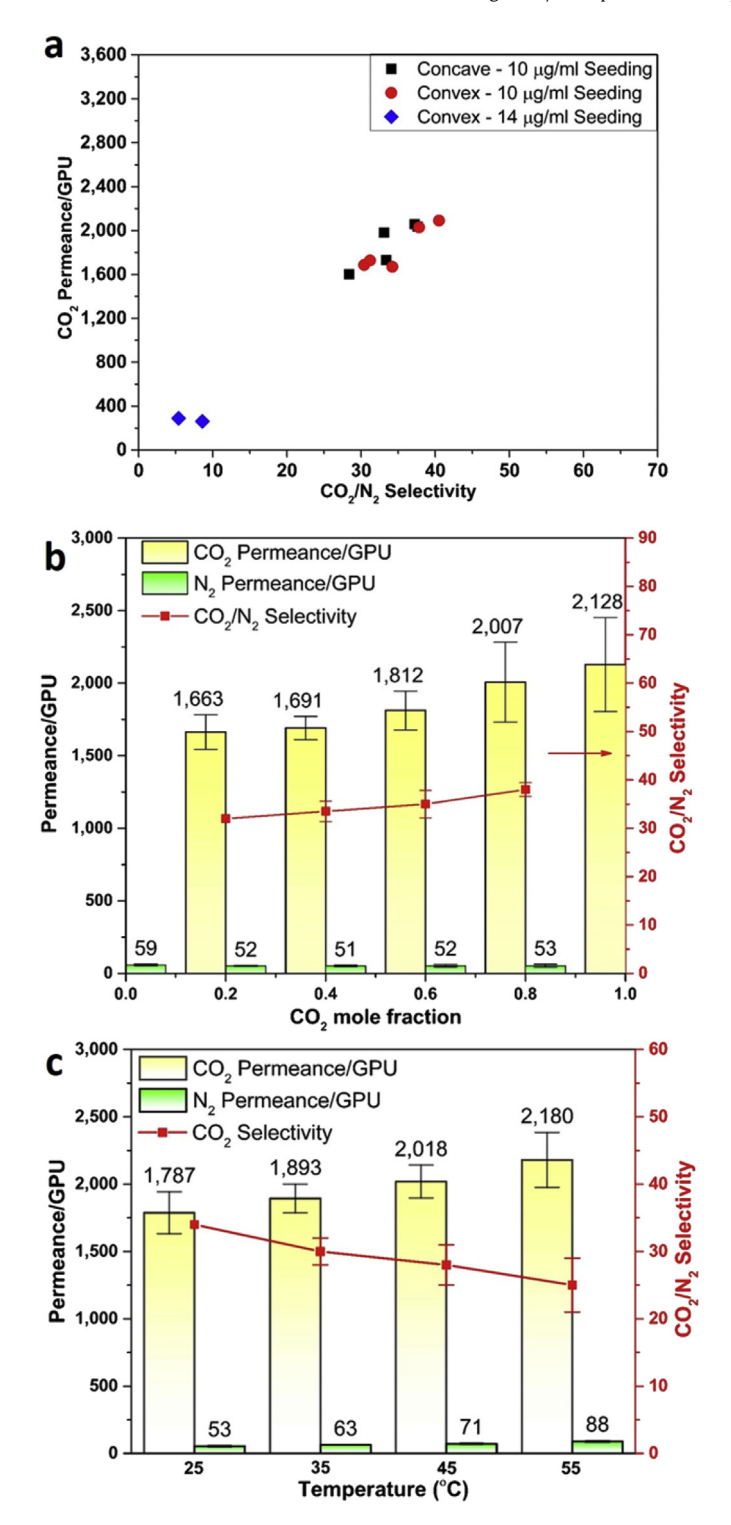


Fig. 7. (a). CO_2/N_2 gas transport results of zeolite membranes from roll-to-roll setup; effect of (b) different CO_2 mole fraction in feed gas and (c) temperature on gas separation performance.

4 Discussion

In this study, we have adapted our previously reported rapid growth process of zeolite synthesis to a membrane that undergoes flexing during the synthesis process [13,15]. This was accomplished by assembling a roll-to-roll assembly, in which a seeded PES support is rolled slowly through an activated gel (Figs. 1 and 2).

Two possible geometries were explored, one that would be subjected to a compressive stress (convex) and the other to tensile stress (concave) upon completion of the membrane growth and subsequent flattening (Fig. 3). A third sample involved a higher loading seed sample and was grown in the convex geometry. In the latter case, a continuous zeolite membrane grows on top of the PES support, as shown in Fig. 6.

For these continuous zeolite films grown on top of PES, the compressive stress upon flattening leads to multiple parallel cracks (Fig. 6b). Strains can arise in the zeolite film due to material growing into the grain boundaries of the film, which cannot be accommodated upon flattening. In some of these films, we have also noted wedge cracks, indicating shear forces in the film [18]. There are many studies of the mechanical stability of continuous inorganic layers deposited on polymers [19-24]. These are technologically important materials, primarily used as gas barriers in pharmaceutical and food packaging industries, and also an emerging application in design of organic light emitting diodes and batteries. All these films are susceptible to cracking under mechanical bending. Parallel cracks like the ones shown in Fig. 6b are also noted on 100 nm thick silicon oxynitride on polyethylene naphthalate (PEN) and polyethylene terephthalate (PET) (125–130 microns) films [20]. The two explanations for these cracks are as follows [25]. First, during synthesis, due to thermal mismatch, the inorganic layer can be under compressive stress and the polymer layer under tensile stress. In order to relieve the stress, the polymer layer cracks open, and that causes the inorganic film to crack. A second scenario is that the film is under compressive stress, and to reduce the strain energy, the film buckles and then cracks follow. The polymer layer is not influenced. Fig. 6c shows that in the case of zeolite grown on top of the film, the PES layer is intact, suggesting that the compressive stress in the zeolite film is leading to cracking.

For the zeolite membranes grown within the PES pores, in both convex (compressive) and concave (tensile) growth, no obvious defects were noted on the membrane surfaces (Fig. 5). Upon dissolution of the PES, large, continuous films of connected zeolite crystals was observed. The thicknesses of the inorganic membrane is higher in the concave than in the convex sample (Fig. 5). The other difference is that in the case of the concave growth, there are only few crystals on the top surface, whereas in the convex growth, the surface layer consists of many more particles.

In order to get satisfactory transport properties, the membranes were coated with a 200–300 nm layer of PDMS. PDMS is expected to only fix mesoporous defects, not penetrate into microporous zeolite pores, because PDMS monomer has molecular size of 0.80 nm, which is larger than pore size of zeolite Y (0.74 nm) [26]. As long as the zeolite membrane is formed within the PES pores, the $\mathrm{CO}_2/\mathrm{N}_2$ transport properties were similar (Fig. 7a). Since PDMS

Table 1Gas separation performance change with different bending diameters for PDMS coated convex membranes.

Bend direction	Diameter/cm	CO ₂ Permeance/GPU	N ₂ Permeance/GPU	CO ₂ /N ₂ selectivity
As-synthesized (Convex)	_	2030	54	38
Bending in	2.5	1860	51	37
	1.3	1408	1094	1
Bending out	2.5	1617	45	36
	1.3	1666	1421	1

layer alone has CO_2/N_2 selectivity of ~10, reported CO_2/N_2 selectivity of 34–35 is attributed to the zeolite layer. However, for the zeolite membrane grown on top of the PES, the cracks are too large for PDMS to have any effect, and the transport properties are seriously compromised (Fig. 7a).

Typically, most inorganic oxides grown on substrates are under compressive stress, and the stress can be reduced by formation of cracks [27,28]. This is what is happening with the continuous zeolite film on top of the PES. What is of interest is the stability of the zeolite film that is grown under stress within the PES. As is evident from the SEM data in Fig. 5, once the PES is dissolved, the zeolite film is porous, with the pore structure arising due to the network of PES that exists within the membrane. Porous films are generally under tensile stress, as compared to dense films, which typically are under compressive stress. Growth of zinc oxide films on flexible glass substrates under strain conditions were comparable in reliability as compared to those grown without strain [29].

The literature on inorganic films on polymer substrates provide some insight as to the observed mechanical stability. Significant lowering in crack density as a function of bending radius for metal oxide films on polymers is observed if the metal oxide is further coated with another polymer layer [23,30]. Two explanations have been suggested for the enhanced mechanical ruggedness [19,20,31,32]. First is that the top polymer coat is shifting the stress neutral plane to the lower inorganic layer, thereby decreasing the stress felt by this film. It is not clear at this stage if the stress neutral plane is relevant in relieving the stress for the zeolite/PES membranes. The second explanation relates to the top polymer layer penetrating into the cracks in the inorganic film, thereby increasing the radius of the defect tip. In the case of the zeolite film within the PES, the PES microstructure can be visualized as penetrating within the zeolite network, providing opportunities for relieving the stress within the growing zeolite film, and is the more likely explanation of the mechanical stability. However, as Table 1 shows, there is a limit to the bending, with the membranes failing once bent around a radius of 1.3 cm, either bending in or bending out. For inorganic ZnO films on PES substrates, a difference in mechanical property was noted between bending in and out [33].

Most importantly, the success of this type of zeolite membrane growth paves the way for a continuous process, mimicking the very successful polymer membrane growth, extensively realized for several technological applications. The challenge now is to design a reactor where the optimized aluminosilicate gel solution is continuously fed, so that zeolite growth activity is maintained over longer periods, and the process of zeolite membrane growth can be made continuous for long lengths of zeolite-polymer membranes. Another challenge is to understand why the permeance slowly decreases with time, though the selectivity remains unchanged.

5. Conclusion

Zeolite membrane samples were made while rolling through a heated aluminosilicate gel. The process was completed in 1 h, with the zeolite growing within the pores of the PES support or on top of the support depending on the nanozeolite seed levels. Membranes in both convex and concave geometry were grown. With PDMS coating, zeolite membranes grown within the PES support have $\rm CO_2$ permeance of 1880 GPU and $\rm CO_2/N_2$ selectivity of 34. However, if zeolite membranes were grown on top of the PES support, they cracked under compressive stress. Demonstration of zeolite membrane under roll-to-roll synthesis conditions opens up the potential of low cost manufacture of zeolite membranes.

Author contributions

This manuscript is based on the PhD thesis of Bo Wang, who did the bulk of the work. Eric Jackson designed the electrical component of the reactor and Jerry Hoff (now deceased) designed the mechanical part of the reactor. The paper was written through contributions of all authors. All authors have given approval to the final version of the manuscript.

Funding sources

This work is funded by The U. S. Department of Energy under Award Number DE-FE0007632. However, any opinions, findings, conclusions, or recommendations expressed herein are those of the author(s) and do not necessarily reflect the views of the DOE.

Financial interest

The authors declare no competing financial interest.

References

- [1] C.E. Powell, G.G. Qiao, J. Membr. Sci. 279 (2006) 1-49.
- [2] L.M. Robeson, J. Membr. Sci. 320 (2008) 390-400.
- [3] R. Krishna, J.M. van Baten, J. Membr. Sci. 360 (2010) 323-333.
- [4] J. Caro, M. Noack, P. Kölsch, R. Schäfer, Microporous Mesoporous Mater. 38 (2000) 3–24.
- [5] J. Gascon, F. Kapteijn, B. Zornoza, V. Sebastián, C. Casado, J. Coronas, Chem. Mater. 24 (2012) 2829–2844.
- [6] A. Tavolaro, E. Drioli, Adv. Mater. 11 (1999) 975-996.
- K. Sawamura, T. Furuhata, Y. Sekine, E. Kikuchi, B. Subramanian, M. Matsukata, ACS Appl. Mater. Interfaces 7 (2015) 13728–13730.
- [8] T.C. Merkel, H. Lin, X. Wei, R. Baker, J. Membr. Sci. 359 (2010) 126-139.
- [9] N. Kaihovirta, T. Mäkelä, X. He, C.-J. Wikman, C.-E. Wilen, R. Österbacka, Org. Electron 11 (2010) 1207—1211.
- [10] H. Yang, P. Jiang, Langmuir 26 (2010) 13173-13182.
- [11] R.R. Søndergaard, M. Hösel, F.C. Krebs, J. Polym. Sci. Part B Polym. Phys. 51 (2013) 16–34.
- [12] M. Cakmak, S. Batra, B. Yalcin, Polym. Eng. Sci. 55 (2015) 34–46.
- [13] M. Severance, B. Wang, K. Ramasubramanian, L. Zhao, W.S.W. Ho, P.K. Dutta, Langmuir 30 (2014) 6929–6937.
- [14] B. Wang, C. Sun, Y. Li, L. Zhao, W.S.W. Ho, P.K. Dutta, Microporous Mesoporous Mater. 208 (2015) 72–82.
- [15] B. Wang, W.S.W. Ho, J.D. Figueroa, P.K. Dutta, Langmuir 31 (2015) 6894-6901.
- [16] S. Chakraborty, M. Severance, T. Young, P.K. Dutta, J. Phys. Chem. C 119 (2015) 15491–15499.
- [17] B.A. Holmberg, H. Wang, J.M. Norbeck, Y. Yan, Microporous Mesoporous Mater. 59 (2003) 13–28.
- 18] A. Atkinson, Br. Ceram. Proc. 54 (1995) 1–14.
- [19] Y. Leterrier, Prog. Mater. Sci. 48 (2003) 1-55.
- [20] S. Grego, J. Lewis, E. Vick, D. Temple, Thin Solid Films 515 (2007) 4745–4752.
- [21] Y. Leterrier, L. Médico, F. Demarco, J.-A.E. Månson, U. Betz, M.F. Escolà, M. Kharrazi Olsson, F. Atamny, Thin Solid Films 460 (2004) 156–166.
- [22] W.-P. Vellinga, A. Fedorov, J.T. De Hosson, Thin Solid Films 517 (2008) 841–847.
- [23] Y. Zhang, R. Yang, S.M. George, Y.-C. Lee, Thin Solid Films 520 (2011) 251–257.
- [24] D.C. Miller, R.R. Foster, Y. Zhang, S.-H. Jen, J.A. Bertrand, Z. Lu, D. Seghete, J.L. O'Patchen, R. Yang, Y.-C. Lee, S.M. George, M.L. Dunn, J. Appl. Phys. 105 (2009) 093527.
- [25] A.Z. Kattamis, K.H. Cherenack, I.-C. Cheng, K. Long, J.C. Sturm, S. Wagner, in: Symp. M – Mater. Technol. Flex. Conform. Stretchable Sens. Transistors, 1078, 2008, pp. 16–21.
- [26] W.V. Chiu, I.-S. Park, K. Shqau, J.C. White, M.C. Schillo, W.S.W. Ho, P.K. Dutta, H. Verweij, J. Membr. Sci. 377 (2011) 182–190.
- [27] H.K. Pulker, Vak. Forsch. Prax. 11 (1999) 42-47.
- [28] G.C.A.M. Janssen, Thin Solid Films 515 (2007) 6654–6664.
- [29] C.-Y. Peng, T.P. Dhakal, S.M. Garner, P. Cimo, S. Lu, C.R. Westgate, IEEE Trans. Device Mater. Reliab. 14 (2014) 121–126.
- [30] V. Zardetto, T.M. Brown, A. Reale, A. Di Carlo, J. Polym. Sci. Part B Polym. Phys. 49 (2011) 638–648.
- [31] R.S. Dahiya, S. Gennaro, IEEE Sens. J. 13 (2013) 4030–4037.
- [32] P. Zinck, M.F. Pay, R. Rezakhanlou, J.F. Gerard, J. Mater. Sci. 34 (1999) 2121–2133.
- [33] Z.-L. Tseng, Y.-C. Tsai, S. Wu, Y.-D. Juang, S.-Y. Chu, ECS J. Solid State Sci. Technol. 2 (2013) P16—P19.